

Electronic structures of tungsten surfaces and total-energy distributions of the field-emission current

M. J. G. Lee* and Z. A. Ibrahim

Department of Physics, University of Toronto, 60 Saint George St., Toronto, Ontario, M5S 1A7, Canada

(Received 11 February 2004; published 30 September 2004)

The surface densities of states (SDOS) and the total energy distributions (TED) of the field emission current from low-index tungsten-vacuum interfaces are deduced from *ab-initio* calculations of their electronic structures. While all of the components in a plane-wave expansion of the transverse wave function of an electron state at the interface make an important contribution to the SDOS, the dominant contribution to the field emission current comes from the zero-momentum component, whose size depends on the symmetry of the electron state. Calculations of the TEDs in field emission from the (100), (110), and (111) surfaces of tungsten are used to interpret features observed in the experimental TEDs and to extract information about the electronic structures of the surfaces.

DOI: 10.1103/PhysRevB.70.125430

PACS number(s): 73.20.At, 73.40.-c, 79.70.+q

I. INTRODUCTION

In a field emission experiment, a strong electric field is applied to the oriented single crystal that constitutes the tip (the approximately hemispherical apex of radius approximately $0.1 \mu\text{m}$) of an etched wire sample that is welded to a wire loop and mounted in an ultra-high vacuum enclosure. The tip is made atomically clean and annealed by passing a current through the loop to flash it to white heat. Electrons field emitted from the desired facet of the tip are selected by a probe hole, and the total energy distribution (TED) of the emission current is measured by means of an electron energy analyzer. Field emission involves quantum mechanical tunneling through the potential barrier at the metal-vacuum interface. The tunneling barrier selects strongly for electrons in states of small transverse momentum, so the emission current is dominated by electron states that are close to the symmetry point $\bar{\Gamma}$, which is the center of the surface Brillouin zone (SBZ).

While measurements of the TED in field emission can yield information about the occupied electron states at the surfaces of metals, the interpretation of the data has been the subject of much discussion. In a pioneering calculation of the field emission current from $W(100)$, Penn and Plummer¹ stated that the TED is a measure of the surface density of states (SDOS) in the vicinity of $\bar{\Gamma}$. An experimental study of angle-resolved photoemission and field emission from $W(100)$ ² identified three bands of surface resonances below the Fermi level, but the accompanying non-self-consistent calculation failed to account for the observed symmetry of the upper resonance (the Swanson hump). Posternak *et al.*,³ in a self-consistent calculation of the electronic structure of a $W(100)$ slab, were the first to observe a feature corresponding to the Swanson hump.⁴ Subsequently, several workers have reported self-consistent electronic structure calculations for $W(100)$ ⁵⁻⁷ and $W(111)$.⁸ Features in the experimental TEDs of the field emission current⁸⁻¹⁰ have been interpreted by comparing them with calculated surface densities of states in the vicinity of $\bar{\Gamma}$.

Modinos and Nicolaou¹¹ used a transfer Hamiltonian approach to calculate the field emission current from semi-infinite $W(100)$ and $W(110)$ crystals, assuming a lattice of muffin-tin potentials terminated abruptly at the surface. They pointed out that, for each electron state of the metal, only the component corresponding to $\mathbf{g}_S=0$ (where \mathbf{g}_S is a surface reciprocal lattice vector) in a plane wave expansion of the transverse wave function at the surface contributes appreciably to the tunneling current.

Modinos¹² reported calculations of the TEDs in field emission from $W(100)$ and $W(110)$, based on Posternak's self-consistent potential, in which only the zero-momentum components of the transverse wave functions contribute to the tunneling current. He noted that a feature corresponding to the Swanson hump in field emission from $W(100)$ appears only in TEDs deduced from self-consistent potentials.

Plummer *et al.*^{9,10,13} measured the enhancement factors in field emission (defined as the ratio of the experimental TED of the field emission current divided by the TED calculated in the free-electron approximation) for several low-index surfaces of tungsten at 78 K. Subsequent measurements⁸ of the enhancement factors in field emission from $W(100)$ and $W(111)$ at room temperature were found to be in good overall agreement with the 78 K data. However, a calculation of the k -resolved SDOS¹⁴ failed to predict correctly the relative strengths of the experimentally-observed peaks of different symmetries.

In this paper we report revised experimental enhancement factors for field emission from $W(100)$ and $W(111)$ at room temperature, involving improved corrections for the dead time of the photomultiplier, as well as new results for field emission from $W(110)$ at room temperature. We describe how standard techniques for calculating the electronic structures of metals can be adapted to calculate the TED of the field emission current at a low-index metal-vacuum interface. The interface is represented by a supercell whose electronic structure is calculated on the basis of density functional theory (DFT) by the full-potential linearized augmented plane wave (FP-LAPW) method. The contribution of each electron state to the TED is expressed as the

product of a supply function (the product of the zero-momentum component of the SDOS and the velocity with which the electron approaches the surface potential barrier) and the transmission coefficient of the surface potential barrier. Because the higher momentum ($\mathbf{g}_S \neq 0$) components in a plane wave expansion of the transverse wave function are strongly attenuated by the surface potential barrier, those electron states for which the zero-momentum ($\mathbf{g}_S=0$) component of the transverse wave function is large make the dominant contribution to the field emission current. It is shown that the size of the zero-momentum component of the transverse wave function depends on the symmetry of the electron state. The calculated TEDs are found to be in good overall agreement with the experimental data. Significant broadening of the experimental peaks relative to the calculated peaks is consistent with lifetime broadening due to defect scattering.

This paper is organized as follows. In Sec. II, we show how the tetrahedron method for evaluating Brillouin zone integrals in density of states calculations can be adapted to calculate the TED in field emission at a metal-vacuum interface, taking into account the normal velocities of the electrons at the surface potential barrier and including only the zero-momentum components of the transverse wave functions. In Sec. III, the TEDs in field emission from the (100), (110) and (111) surfaces of tungsten are calculated and used to interpret features observed in the experimental TEDs. The results and conclusions of this work are summarized in Sec. IV.

II. THEORY AND COMPUTATIONAL DETAILS

A. Zero-momentum component of the layer DOS

The metal-vacuum interface is described by a supercell containing 13 layers of tungsten atoms [9 layers for $W(110)$], surrounded by an atom-free region of equal volume to represent the vacuum. The electronic structure of the interface is calculated self-consistently by the FP-LAPW method using WIEN2K.¹⁵ Exchange and correlation are treated in the generalized-gradient approximation (GGA).¹⁶ Relativistic corrections, including the spin-orbit interaction, are included in the calculation.

In the FP-LAPW method, the metal is divided into a *spherical region* that consists of nonintersecting spheres centered on each atomic site, and the complementary *interstitial region*. Inside the spherical region the wave functions are expanded as linear combinations of radial functions multiplied by spherical harmonics, while in the interstitial region they are expanded as linear combinations of plane waves. We introduce two planes normal to the surface to characterize the metal-vacuum interface. The *surface plane* ($z=z_S$) contains the centers of the atoms in the outer layer, and the *interface plane* ($z=z_0$) represents the electrical surface of the metal.

On the metal side of the interface plane ($z < z_0$) the applied electrostatic field is assumed to be fully screened out by the valence electrons, so the potential is the self-consistent potential of a half-plane of atoms. On the vacuum

side of the interface plane ($z > z_0$) the potential is assumed to be a superposition of the image potential $-e^2/[4(z-z_0)]$ and the potential $-eF(z-z_0)$ due to the applied electrostatic field F , where e is the magnitude of the electronic charge. The image potential approximation fails at less than some minimum distance z_C from the interface plane, so in the range $z_0 < z \leq z_C$ the potential is taken to be constant and equal to the mean potential in the interface plane (V_S). Outside the metal, therefore, the potential can be written (in egs units) as

$$V(z) = V_S, \quad \text{for } z_0 < z \leq z_C,$$

$$V(z) = (E_F + \Phi) - e^2/[4(z-z_0)] - eF(z-z_0), \quad \text{for } z > z_C, \quad (1)$$

where E_F is the Fermi energy and Φ is the work function of the emitting surface. The distance z_C is chosen so that the potential is a continuous function of z . Experimental studies of field and photofield emission from $W(100)$ ¹ and $W(111)$ ¹⁷ have shown that the applied electric field is too weak to have a significant effect on the energies of surface states and surface resonances.

Kohn and Lang¹⁸ have shown, on the basis of jellium calculations, that the electrical surface of a metal coincides with the centroid of the charge induced by the external electric field, and they suggested that it also coincides with the image plane. Forbes,¹⁹ using an array model for the close-packed surfaces of various metals, demonstrated that in all cases the electrical surface is located at approximately one half of the nearest neighbor distance from the surface plane. However, the array model cannot be used to make an accurate determination of the electrical surface because, as pointed out by Forbes, there is no realistic way to quantify the uncertainties arising from the limitations of the model itself.

In the present calculations the interface plane was taken to be sufficiently far from the surface plane that the potential does not vary greatly over the interface plane, but sufficiently close that all of the electronic states whose contributions to the emission current are to be calculated have positive kinetic energies at the interface plane. We find that when these two conditions are satisfied, the distance between the interface plane and the surface plane is approximately one half of the nearest neighbor distance, so the interface plane is close to the electrical surface. Provided that the interface plane is close to the electrical surface, it is a feature of our model that the shape of the surface potential barrier [Eq. (1)], and hence its transmission coefficient, is independent of the choice of z_0 .

The wave function $\psi_{\mathbf{k}}(\mathbf{r})$ is separable in the region $z > z_0$. While the translational symmetry of the normal wave function is broken at the interface plane, the translational symmetry of the transverse wave function is preserved. In the region $z_0 < z \leq z_C$, the transverse wave function at \mathbf{r} can be expressed as a sum, over the surface reciprocal lattice vectors \mathbf{g}_S , of plane waves of the form $\exp[i(\mathbf{k}_{\parallel} + \mathbf{g}_S) \cdot \mathbf{r}]$, where \mathbf{k}_{\parallel} is the transverse wave vector of the electron state. As the transverse wave vector \mathbf{k}_{\parallel} and the total energy E are conserved at

the metal-vacuum interface, the normal kinetic energy of the plane wave component $\exp[i(\mathbf{k}_{\parallel} + \mathbf{g}_S) \cdot \mathbf{r}]$ in the region $z_0 < z < z_C$ is given by

$$W = E - V_S - \hbar^2(\mathbf{k}_{\parallel} + \mathbf{g}_S)^2/(2m), \quad (2)$$

where V_S is the mean potential in the interface plane.

With increasing transverse momentum $(\mathbf{k}_{\parallel} + \mathbf{g}_S)$, the transmission coefficient of the surface potential barrier $D(W)$ decreases exponentially. In the range of electrostatic fields used in a typical field emission experiment, the transmission coefficient of the surface potential barrier at $W(100)$ for an electron state at \bar{X} (the point on the boundary of the SBZ closest to $\bar{\Gamma}$) is smaller than that for an electron state of the same energy at $\bar{\Gamma}$ by a factor of 10^{-17} . It follows that the field emission current is dominated by the component in the plane wave expansion for which $\mathbf{g}_S = 0$. Therefore, in calculating the contribution of electron states at \mathbf{k}_{\parallel} to the field emission current, it is an excellent approximation to neglect all of the higher momentum components ($\mathbf{g}_S \neq 0$) and to include only the ($\mathbf{g}_S = 0$) component,¹¹ which we call the *zero momentum component*. This is the approximation on which the present work is based.

The transverse component of $\psi_k(\mathbf{r})$ is of the Bloch form with wave vector \mathbf{k}_{\parallel} , so in any transverse plane the function $\psi_k(\mathbf{r}) \exp(-i\mathbf{k}_{\parallel} \cdot \mathbf{r})$ has the same periodicity as the lattice. The zero momentum component of $\psi_k(\mathbf{r})$ in any given plane can be calculated by integrating $\psi_k(\mathbf{r}) \exp(-i\mathbf{k}_{\parallel} \cdot \mathbf{r})$ over one lattice cell within that plane. The fractional contribution of the zero-momentum component of $\psi_k(\mathbf{r})$ to the density of states is therefore

$$F_k = \left[\int \psi_k(\mathbf{r}) \exp(-i\mathbf{k}_{\parallel} \cdot \mathbf{r}) \mathbf{d}s \right] \left[\int \psi_k(\mathbf{r}) \times \exp(-i\mathbf{k}_{\parallel} \cdot \mathbf{r}) \mathbf{d}s \right] \Bigg/ \left[S \int \psi_k(\mathbf{r})^* \psi_k(\mathbf{r}) \mathbf{d}s \right],$$

where each of the integrals is evaluated over one lattice cell (of area S) within the plane.

The results of the present work are based on semirelativistic calculations of the surface densities of states in which the spin-orbit interaction is taken into account. However, spin-orbit wave functions are not currently obtainable from WIEN2K, so we used non-spin-orbit wave functions to evaluate the zero-momentum fractions F_k . Since the dominant features in the surface density of states, including the Swanson hump on $W(100)$, appear even when the spin-orbit interaction is neglected, the use of non-spin-orbit wave functions to evaluate F_k is not expected to reduce significantly the accuracy of our final results.

B. TED of the field emission current

The TED $j(E)$ is the derivative of the emission current density with respect to total energy E . The field emission TED calculated in the free-electron approximation, $j_0(E)$, is dominated at low energy by an exponential decrease due to the transmission coefficient of the surface potential barrier,

and at high energy by an exponential decrease due to the Fermi-Dirac distribution function, resulting in a peak at the Fermi energy. As a first step in analyzing experimental field emission data, it is convenient to remove the exponential energy dependencies below and above E_F by dividing the measured TED $j(E)$ by $j_0(E)$. The ratio $j(E)/j_0(E)$ is called the *experimental enhancement factor*.

We calculated $j_0(E)$ from^{12,20}

$$j_0(E) = [me/(2\pi^2\hbar^3)]f(E) \int_{V_S}^E \mathbf{d}W D(W), \quad (4)$$

where m is the free-electron mass, e is the magnitude of the electronic charge and $f(E)$ is the Fermi-Dirac distribution function. To determine $D(W)$, the transmission coefficient of the surface potential barrier, the normal wave function corresponding to normal energy W was evaluated by integrating the one-dimensional Schrodinger equation across the surface potential barrier [Eq. (1)] using an exact numerical technique due to Vigneron and Lambin.^{22,23} The charge fluxes on the two sides of the barrier were calculated from the Wronskians of the normal wave function, and $D(W)$ was evaluated from the ratio of fluxes.

The WIEN2K program *tetra* calculates the surface density of states by dividing the Brillouin zone into a large number of tetrahedra of equal volume and evaluating

$$\text{SDOS}(E) = \sum_{\kappa} \sum_i \text{SDOS}_{\kappa,i}(E), \quad (5)$$

where the distribution $\text{SDOS}_{\kappa,i}(E)$ is the contribution of band i in tetrahedron κ to the density of states in the surface layer for a single direction of electron spin.²¹ In the K -SDOS approximation the electron velocities are neglected and the transmission coefficients of all plane wave components of the transverse wave function are assumed to be equal. The enhancement factor calculated in this approximation is called the *k-resolved surface density of states*:

$$K\text{-SDOS}(E) = \left[\sum_{\kappa} \sum_i \text{SDOS}_{\kappa,i}(E) D(W_{\kappa,i}) \right] \Bigg/ D(E). \quad (6)$$

K -SDOS(E) was calculated using a modified version of *tetra* in which, in the sum over tetrahedra and bands, $\text{SDOS}_{\kappa,i}(E)$ is replaced by $\text{SDOS}_{\kappa,i}(E)[D(W_{\kappa,i})/D(E)]$. The normal kinetic energy $W_{\kappa,i}$ and the total energy $E_{\kappa,i}$ of band i in tetrahedron κ were taken to be those of the electron state at the centroid of the tetrahedron. In the K -SDOS approximation, the relationship between $W_{\kappa,i}$ and $E_{\kappa,i}$ in the region $z_0 < z < z_C$ that applies for $\mathbf{g}_S = 0$, $W_{\kappa,i} = E_{\kappa,i} - V_S - \hbar^2\mathbf{k}_{\parallel}^2/(2m)$, is used for all \mathbf{g}_S . We evaluated $D(W_{\kappa,i})$ from the normal wave function of energy $W_{\kappa,i}$ as described above.

In the present calculations of the TEDs of the field emission current from low-index metal-vacuum interfaces, both the normal velocities of the electrons at the surface potential barrier and the attenuation of the higher-momentum components of the transverse wave functions are taken into account. The TEDs were calculated from

$$j_S(E) = 2ef(E) \sum_{\kappa} \sum_i \text{SDOS}_{\kappa,i}(E) F_{\kappa,i} v_{\kappa,i} D(W_{\kappa,i}), \quad (7)$$

where the factor of two takes into account the two directions of electron spin. The zero-momentum contribution to the SDOS in the interface plane is obtained by multiplying $\text{SDOS}_{\kappa,i}(E)$, the density of states evaluated in the surface plane, by

$$F_{\kappa,i} = \frac{\left[\int \psi_{\kappa,i}(\mathbf{r}) \exp(-i\mathbf{k}_{\parallel} \cdot \mathbf{r}) d\mathbf{s} \right] \left[\int \psi_{\kappa,i}(\mathbf{r}) \exp(-i\mathbf{k}_{\parallel} \cdot \mathbf{r}) d\mathbf{s} \right]}{\left[S \int \psi_{\kappa,i}(\mathbf{r})^* \psi_{\kappa,i}(\mathbf{r}) d\mathbf{s} \right]}, \quad (8)$$

where each of the integrals in the numerator is evaluated over one lattice cell (of area S) within the interface plane, the integral in the denominator is evaluated over one lattice cell within the surface plane, and $\psi_{\kappa,i}(\mathbf{r})$ is the wave function of the electron state in band i at the centroid of tetrahedron κ . In practice, the integral in the denominator was estimated by averaging $\int \psi_{\kappa,i}(\mathbf{r})^* \psi_{\kappa,i}(\mathbf{r}) d\mathbf{s}$ over three equally-spaced planes that span the surface layer. For the zero momentum components, the relationship between the normal energy $W_{\kappa,i}$ and the total energy $E_{\kappa,i}$ in the region $z_0 < z < z_C$ is $W_{\kappa,i} = E_{\kappa,i} - V_S - \hbar^2 \mathbf{k}_{\parallel}^2 / (2m)$. $v_{\kappa,i} = (2W_{\kappa,i}/m)^{1/2}$ is the normal velocity with which the electron approaches the surface potential barrier. $D(W_{\kappa,i})$ was evaluated from the normal wave function of energy $W_{\kappa,i}$ as described above.

The present calculations are based on supercells that accurately model the surface layers of the metal but under-represent the bulk. Accordingly, the TED of the field emission current calculated from Eq. (7) is denoted $j_S(E)$, where the subscript S denotes a surface contribution. In order to compare the calculated enhancement factors with the experimental enhancement factors, $j_S(E)$ was corrected by adding $j_0(E)$, the bulk contribution estimated from the free-electron model. The good overall agreement between the present results and experiment indicates that the free-electron model provides a satisfactory approximation to the bulk contribution; a more accurate treatment would require a full calculation of the TED in field emission from a semi-infinite lattice.

The TEDs of the field emission current were evaluated by a modified version of *tetra* in which, in the sum over tetrahedra and bands, $\text{SDOS}_{\kappa,i}(E)$ is replaced by $2ef(E) \text{SDOS}_{\kappa,i}(E) F_{\kappa,i} v_{\kappa,i} D(W_{\kappa,i})$. The computational resources needed to evaluate the TEDs were greatly reduced by including in the sum over κ only those tetrahedra whose centroids lie close to $\bar{\Gamma}$. For example, we found that only those tetrahedra whose centroids lie within a sphere of radius 0.3 \AA^{-1} around $\bar{\Gamma}$ ($\sim 30\% \bar{\Gamma}\bar{X}$) make a significant contribution to the field emission current from $W(100)$. Neglecting the tetrahedra outside this range reduces the number of terms in the sum over κ in Eq. (7) by a factor of ten.

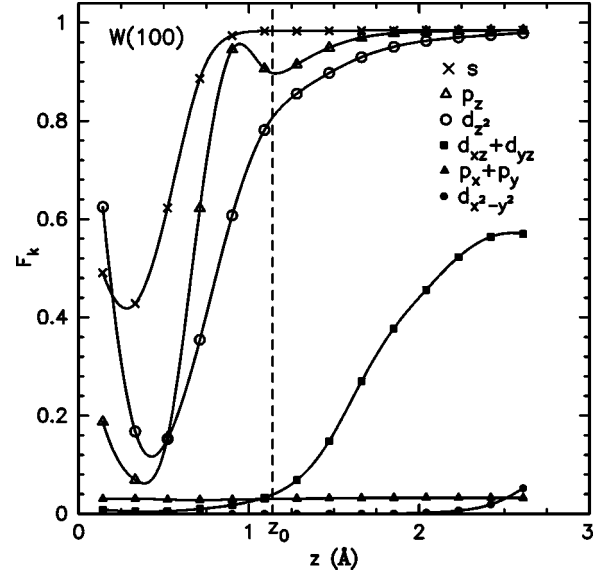


FIG. 1. Fractional contribution of the zero-momentum component of the transverse wave function of a single electron state at $\bar{\Gamma}$ to the density of states in the interface plane at a $W(100)$ -vacuum interface. F_k , defined by Eq. (3), is plotted as a function of the distance between the surface plane and the assumed interface plane for representative states of various symmetries at a $W(100)$ -vacuum interface. z_0 marks the location of the interface plane used in the present work.

III. RESULTS AND DISCUSSION

A. Electron symmetry and the DOS in the interface plane

F_k as defined by Eq. (3) is the zero-momentum fraction of the contribution of the electron state of wave vector \mathbf{k} to the density of states in the given plane. In Fig. 1 the zero-momentum fraction F_k at $W(100)$ is plotted, for electron states of various symmetries at $\bar{\Gamma}$, as a function of the distance between the surface layer and the assumed interface plane.

The common feature of the electronic states at $\bar{\Gamma}$ whose predominant symmetries are s , p_z , and d_z^2 is that in the interface plane the zero-momentum fractions of their transverse wave functions are all close to one. This is illustrated in Fig. 1, where the rapid increase in F_k with distance shows that the higher momentum components of the s -like state decay over a distance of less than 1 \AA from the surface layer, while the higher-momentum components of the p_z and d_z^2 -like states decay over progressively larger distances. If the interface plane is chosen as shown in Fig. 1 (1.14 \AA from the surface plane, which is close to the atomic radius of 1.3 \AA), the zero-momentum fractions in the interface plane for s , p_z , and d_z^2 -like states are all close to one. It follows that, for each of these symmetries, the density of states in the interface plane is dominated by the zero-momentum component.

The common feature of the electron states of symmetries $p_x + p_y$, $d_{xz} + d_{yz}$, $d(x^2 - y^2)$, and dxy at $\bar{\Gamma}$ is that in the interface plane their zero-momentum fractions are small. This is confirmed by Fig. 1, which shows that the higher momentum

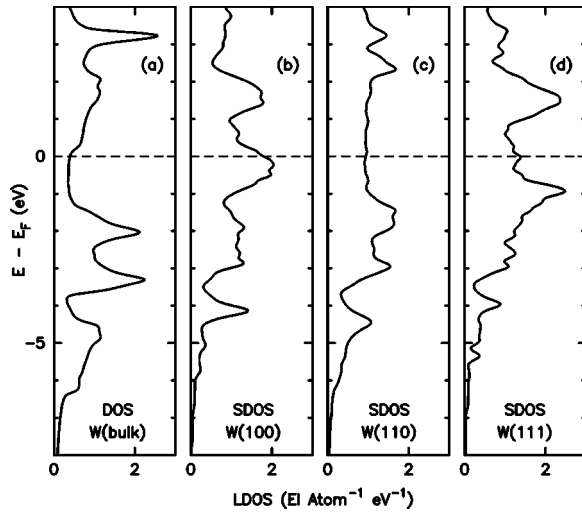


FIG. 2. (a) Calculated density of states of bulk tungsten. (b) SDOS of W(100) calculated from Eq. (5). (c) Calculated SDOS of W(110). (d) Calculated SDOS of W(111).

components of the $dxz+dyz$ -like state decrease very slowly with distance until they reach a plateau, while the higher-momentum components of the $px+py$, $d(x^2-y^2)$, and dxy -like states dominate to very large distances. It will be seen from Fig. 1 that, if the interface plane is chosen as shown (and indeed for any choice of the interface plane that is consistent with the requirements stated in Sec. II A), the zero-momentum fraction in the interface plane for $px+py$, $dxz+dyz$, $d(x^2-y^2)$, and dxy -like states is close to zero. It follows that, even though these states contribute significantly to the K -SDOS, they make only a small contribution to the field emission current.

The transmission properties of the surface potential barrier are such that the TED in field emission is dominated by the zero-momentum fractions of the electron states close to $\bar{\Gamma}$. At the surface of a cubic metal, the zero-momentum fractions of s , p_z , and dz^2 -like states at $\bar{\Gamma}$ are unconstrained by symmetry considerations because their wave functions are uniform in sign over any plane normal to z . However, the zero-momentum fractions of the remaining states are constrained by the symmetry properties of the basis functions. For a (100) surface, the transverse wave functions of $px+py$ and $dxz+dyz$ -like states at $\bar{\Gamma}$ are antisymmetric under inversion [$\psi(-x, -y, z) = -\psi(x, y, z)$], and those of $d(x^2-y^2)$ and dxy -like states at $\bar{\Gamma}$ are antisymmetric under 4-fold rotation about the z axis, so in each case the zero-momentum fraction is zero. For a (110) surface, the transverse wave functions of px , py , dxz , and dyz -like states at $\bar{\Gamma}$ are antisymmetric under inversion, and those of dxy -like states at $\bar{\Gamma}$ are antisymmetric under two-fold rotation about x or y , so in each case the zero-momentum fraction of the transverse wave function is zero. Since the x and y axes are inequivalent, the zero-momentum fractions of $d(x^2-y^2)$ -like states are small but do not vanish. For a (111) surface, it is convenient to take x and y to be oblique coordinates in the hexagonal coordinate system, so that $d(x^2-y^2)$ and dxy are equivalent. Then, as for (100), the zero momentum fractions

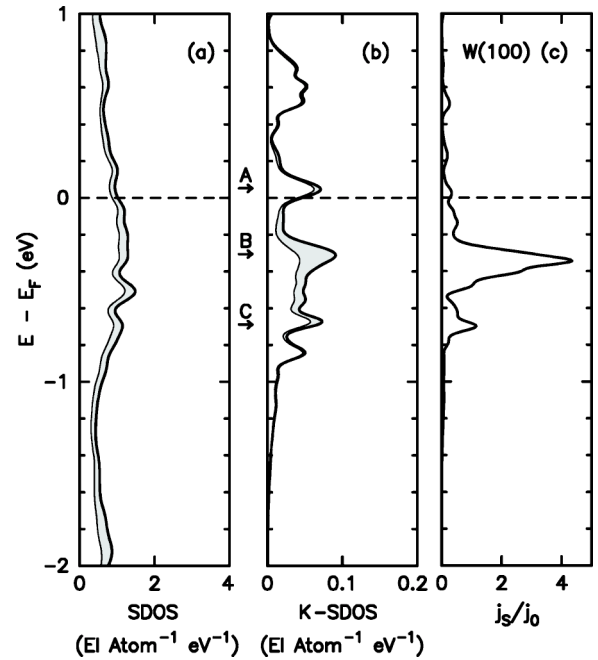


FIG. 3. (a) Calculated SDOS of W(100). (b) K -SDOS of W(100) calculated from Eq. (6). The shaded regions mark the contribution of states of dz^2 symmetry. (c) The enhancement factor for field emission from W(100), calculated from Eqs. (4) and (7). The experimental enhancement factor for field emission from W(100) is shown in Fig. 4(c).

of $px+py$, $dxz+dyz$, and $d(x^2-y^2)+dxy$ -like states at $\bar{\Gamma}$ are zero.

B. Densities of electronic states at low-index surfaces of tungsten

The calculated DOS in the middle layer of each supercell is in good agreement with the DOS obtained from a bulk calculation, confirming that the supercells are sufficiently large to describe the transition from the bulk metal to the surface. Comparing the densities of states in the various layers, the principal difference is between the surface layer and the first sub-surface layer. This difference, which reflects the reduced atomic coordination at the surface, is associated with a redistribution of charge in the surface layer. The calculated surface densities of states at W(100), W(110), and W(111) are shown in Figs. 2(b)–2(d). For comparison, the density of states of bulk tungsten is shown in Fig. 2(a).

The experimental enhancement factor for field emission from W(100) later in Fig. 4(c) shows a strong peak (the Swanson hump⁴) of about 0.35 eV below E_F , and a weak peak about 0.66 eV below E_F . The Swanson hump is hard to see in the SDOS shown in Fig. 3(a), but the calculated K -SDOS in Fig. 3(b) shows three peaks of similar strength, A at 0.04 eV above E_F , the Swanson hump B at 0.31 eV below E_F , and C at 0.69 eV below E_F . In this energy range, the dominant contributions to SDOS and K -SDOS are from d -like states; the contributions of dz^2 -like states are marked by the shaded regions in Figs. 3(a) and 3(b). Peak B is the only peak that is due predominantly to dz^2 -like states. The

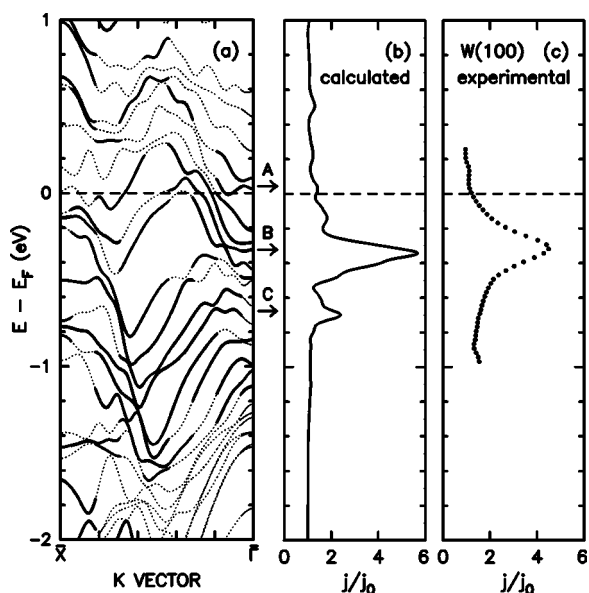


FIG. 4. Field emission from $W(100)$. (a) Surface band structure along $\bar{X}\bar{\Gamma}$. Solid lines mark regions of surface state or surface resonance character, and dotted lines mark regions of bulk or intermediate character. (b) Calculated enhancement factor of the field emission current. (c) Experimental enhancement factor of the field emission current measured at room temperature.

K -SDOS approximation fails to account for the relative strengths of peaks of different symmetries¹⁴ in the experimental enhancement factor [Fig. 4(c)]. It overestimates the contributions of peaks A and C to the emission current because it fails to take into account the normal velocities of the electrons and the greater attenuation of the higher momentum components of the transverse wave functions by the surface potential barrier.

The enhancement factor of the field emission current from $W(100)$ obtained by evaluating Eq. (7) and dividing by $j_0(E)$ is shown in Fig. 3(c). The dominant Swanson peak B centered 0.33 eV below E_F is accompanied by two weaker peaks, A at 0.03 eV above E_F and C at 0.69 eV below E_F . The overall agreement with the experimental enhancement factors measured at 78 K¹⁰ and at room temperature [Fig. 4(c)] is much better than that of the enhancement factor calculated in the K -SDOS approximation. In the following sections, enhancement factors calculated from Eq. (7) are used to interpret features in the TED of the field emission current from low-index surfaces of tungsten.

C. Emission current and electronic structure of $W(100)$, $W(110)$, and $W(111)$

The transition metal tungsten is body-centered cubic, with six valence electrons distributed among the $5d$ and $6sp$ orbitals. The calculated surface energy bands at $W(100)$, $W(110)$ and $W(111)$ are shown in Figs. 4(a), 5(a), and 6(a), respectively. We define a surface energy band as a band that has either surface state character (if a minimum of 75% of the total charge is in the first two layers) or surface resonance character (if the average charge density in the first two layers

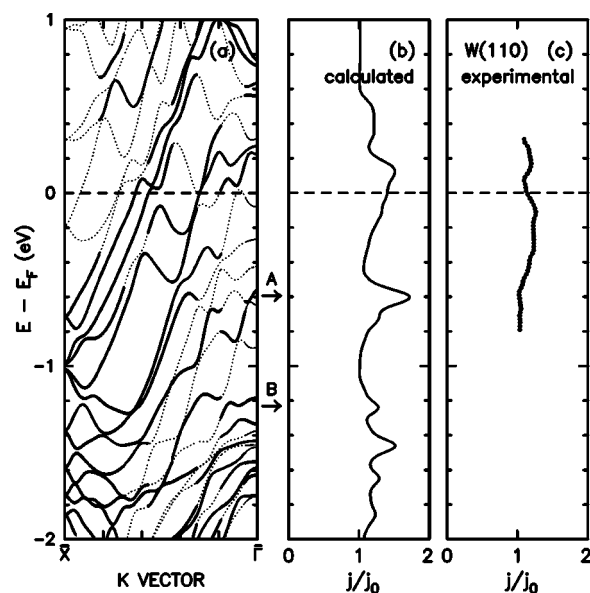


FIG. 5. Field emission from $W(110)$. (a) Surface band structure along $\bar{X}\bar{\Gamma}$. Solid lines mark regions of surface state or surface resonance character, and dotted lines mark regions of bulk or intermediate character. (b) Calculated enhancement factor of the field emission current. (c) Experimental enhancement factor of the field emission current measured at room temperature.

is at least 33% greater than the average in the crystal) over some region of the Brillouin zone. The experimental procedure and the method of data analysis have been described elsewhere.^{8,24}

I. $W(100)$

The geometry of the $W(100)$ -vacuum interface is described by a supercell that consists of six conventional body-centered-cubic unit cells to represent the metal and an atom-free region of equal volume to represent the vacuum. The interface plane is taken to be 1.14 Å from the surface plane. The SBZ is square.

The experimental enhancement factors in field emission from $W(100)$ at 78 K¹⁰ and at room temperature [Fig. 4(c)] show a strong symmetric peak (the Swanson hump) centered about 0.35 eV below E_F . The Swanson hump is consistent with a strong symmetric peak B that appears about 0.33 eV below E_F in the calculated enhancement factor [Fig. 4(b)]. The surface band structure [Fig. 4(a)] shows that peak B is due to a pair of flat dz^2 -like bands that originate as surface states at $\bar{\Gamma}$, 0.29 eV and 0.32 eV below E_F , and disperse towards higher energy as surface resonances. Several other authors^{2,3,5,6,9} have associated peak B with surface states close to $\bar{\Gamma}$. The flat dz^2 -like band of surface states and surface resonances close to $\bar{\Gamma}$ makes a large contribution to the TED in field emission because the zero-momentum fractions of dz^2 -like states are close to one. The experimental dispersion curves deduced from angle-resolved photoemission (ARP) data^{2,25} for $W(100)$ show a band originating at $\bar{\Gamma}$ at the energy of the Swanson hump. The surface band structure in the vicinity of peak B is in qualitative agreement with the

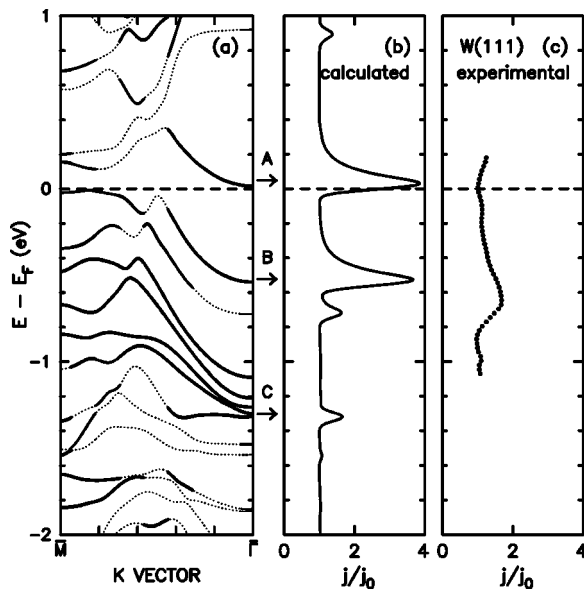


FIG. 6. Field emission from $W(111)$. (a) Surface band structure along $\bar{M}\bar{\Gamma}$. Solid lines mark regions of surface state or surface resonance character, and dotted lines mark regions of bulk or intermediate character. (b) Calculated enhancement factor of the field-emission current. (c) Experimental enhancement factor of the field emission current measured at room temperature.

experimental dispersion curves. However, the observed surface band disperses slightly to higher energy without crossing E_F , while the calculated band crosses E_F at close to $0.3 \bar{\Gamma}\bar{X}$.

The 78 K data show also a weak peak about 0.73 eV below E_F that appears as a poorly-resolved shoulder in the room temperature data. This peak is consistent with the weak peak C in the calculated enhancement factor that is centered about 0.69 eV below E_F . The surface band structure shows that peak C is due to a band of predominantly $dxz+dyz$ -like surface resonances that is flat in the range $0.1 \bar{\Gamma}\bar{X}$ to $0.2 \bar{\Gamma}\bar{X}$ and disperses towards lower energy. The small zero-momentum fractions of $dxz+dyz$ -like states explains why peak C is much weaker than the dz^2 -like peak B (the Swanson hump). The dispersion curves measured by ARP^{2,25} include a band corresponding to peak C that originates at close to $0.2 \bar{\Gamma}\bar{X}$ and that disperses towards lower energy, in agreement with the present results.

By fitting the TED of the emission current calculated in the free electron approximation to the measured TED in the vicinity of the Fermi energy, the width of the resolution function of the energy analyzer can be determined. The full width at half maximum height (FWHM) of the Gaussian resolution function of the energy analyzer was between 10 to 20 meV for the measurements at 78 K, and 56 meV for the room temperature measurements. The FWHMs of the enhancement factors measured at 78 K and at room temperature are almost equal. The calculated enhancement factor, when convolved with the instrumental resolution function appropriate to each data set, is significantly narrower than the measured width. The additional broadening was represented by convolving the calculated distribution with a Lorentzian of ad-

justable width and with the instrumental resolution function. For both data sets, the FWHM of the Lorentzian required to fit the Swanson peak is 85 ± 5 meV, while from the 78 K data the Lorentzian broadening of peak C is 180 ± 10 meV. The Lorentzian broadening is attributed to the lifetime of the final state. The rough proportionality between the Lorentzian broadening and the energy of the field-emitted electron relative to the Fermi level is consistent with the energy dependence of the number of final states available for scattering. The absence of significant temperature dependence in the Lorentzian broadening of the Swanson peak suggests that it is due to defect scattering.

Modinos¹² has calculated the enhancement factor in field emission from $W(100)$ using a lattice of self-consistent muffin-tin potentials, although the potential at the surface was not calculated self-consistently. He found a peak corresponding to the Swanson hump 0.28 eV below E_F , as well as peaks 0.85 eV below E_F and 1.5 eV below E_F . The discrepancy with the energies of peaks obtained in the present work may be due in part to the lack of self-consistency in Modinos' calculation of the potential at the surface.

2. $W(110)$

The geometry of the $W(110)$ -vacuum interface is described by a supercell that consists of nine atomic layers stacked normal to the (110) direction to represent the metal and an atom-free region of equal volume to represent the vacuum. The interface plane is taken to be 1.43 Å from the surface plane. The SBZ is rectangular.

The calculated enhancement factor for field emission from $W(110)$ is plotted in Fig. 5(b). The results of the present calculation, as well as experimental data taken at 78 K¹⁰ and at room temperature [Fig. 5(c)], show little structure over the energy range from 0.3 eV above E_F to 1.6 eV below E_F . The most prominent feature in the calculated enhancement factor is a weak peak A, 0.60 eV below E_F . The band structure in Fig. 5(a) shows that peak A is due to emission from a band of surface resonances of predominantly dxz symmetry, with a small but significant admixture of p_z and dz^2 symmetry. The small size of the calculated peak is due to the small zero-momentum fraction associated with the predominant dxz component of the transverse wave function. The fact that peak A is not clearly seen in the experimental TED can be explained by its inherent weakness if the lifetime broadening is assumed to be comparable to that observed in the same energy range in field emission from $W(100)$.

In the energy range from 1.1 eV to 2.0 eV below E_F , the surface contribution to the enhancement factor at $W(110)$ is predominantly dz^2 -like. The surface band structure in Fig. 5(a) shows that peak B, centered about 1.23 eV below E_F , is due to field emission from a band of surface resonances of dz^2 -symmetry. It seems likely that peak B corresponds to a peak that appears about 1.2 eV below E_F in the experimental data at 78 K.

Modinos¹² calculated the enhancement factor for $W(110)$ based on a lattice of self-consistent potentials. His results show a region of enhanced current 0.1 eV above E_F , decreasing gradually to 1.4 eV below E_F .

3. $W(111)$

The geometry of the $W(111)$ -vacuum interface is described by a supercell that consists of thirteen atomic layers stacked normal to the (111) direction to represent the metal and an atom-free region of equal volume to represent the vacuum. The interface plane is taken to be 1.54 Å from the surface plane. The SBZ is hexagonal.

The calculated enhancement factor for field emission from $W(111)$ is plotted in Fig. 6(b). The surface band structure plotted in Fig. 6(a) shows that the strong asymmetrical peak A centered just above E_F , whose low energy tail extends to slightly below E_F , corresponds to a band of surface resonances predominantly of dz^2 symmetry that originates at $\bar{\Gamma}$ just above E_F and disperses towards higher energy to approximately $0.45 \bar{\Gamma} \bar{M}$. In field emission data it is difficult to identify a peak that lies very close to E_F because of the proximity of the peak at E_F that is due to the cutoff of the Fermi-Dirac distribution. Nevertheless, the room temperature data in Fig. 6(c) show an increase in the experimental enhancement factor just above E_F that is consistent with peak A.

The surface band structure of $W(111)$ in Fig. 6(a) shows that the strong asymmetrical peak B corresponds to a band of surface resonances of dz^2 symmetry that originates at $\bar{\Gamma}$ about 0.53 eV below E_F and disperses towards higher energy to approximately $0.5 \bar{\Gamma} \bar{M}$. The enhancement factors measured at 78 K¹⁰ and at room temperature [Fig. 6(c)] both show strongly asymmetric peaks over the same energy range. However, the maxima of the experimental peaks are 0.75 eV and 0.65 eV below E_F (significantly below the calculated peak). The surface band structure predicts an additional dz^2 -like band originating at $\bar{\Gamma}$ about 0.72 eV below E_F , which might appear to be in better agreement with the experimental data. However, this band is predominantly of bulk character, and its contribution to the calculated emission current is weak because the wave function amplitudes are small in the interface plane.

Peak B in the calculated enhancement factor, when convolved with the instrumental resolution function, is significantly narrower than the corresponding peaks in the experimental data at 78 K and at room temperature. The additional broadening of the room temperature data was determined by convolving the calculated distribution with a Lorentzian of adjustable width and with the instrumental resolution function. The FWHM of the Lorentzian broadening required to fit the room temperature peak is 180 ± 10 meV. While a quantitative analysis of the 78 K data was not undertaken because of uncertainty in extracting the peak width, the Lorentzian broadening is similar to that observed in the same energy range in field emission from $W(100)$.

A weak asymmetrical peak C appears in the calculated enhancement factor [Fig. 6(b)] about 1.3 eV below E_F . The surface band structure shows that peak C is due to a group of surface resonance bands close to $\bar{\Gamma}$ that are predominantly of $d(x^2-y^2)+dxy$ symmetry with a dz^2 admixture. The $d(x^2-y^2)+dxy$ states make a large contribution to the K -SDOS, but they make only a small contribution to the

TED in field emission because their zero-momentum fractions in the interface plane are small. Peak C with strong lifetime broadening may account for the broad peak that appears in the 78 K data about 1.4 eV below E_F .

IV. CONCLUSIONS

In the interface plane, the transverse wave function of each electron state can be expressed as a sum over plane waves $\exp[i(\mathbf{k}_{\parallel} + \mathbf{g}_{\text{S}}) \cdot \mathbf{r}]$, where \mathbf{g}_{S} is a surface reciprocal lattice vector. While the higher-momentum ($\mathbf{g}_{\text{S}} \neq 0$) components contribute to the SDOS and K -SDOS, only the zero-momentum ($\mathbf{g}_{\text{S}} = 0$) component contributes significantly to the TED of the field emission current. This is because the higher momentum components have large transverse energies and correspondingly small normal energies, so they are strongly attenuated by the surface potential barrier.

The contribution of each electron state to the TED in field emission is proportional to its zero-momentum fraction (the fractional contribution to the SDOS in the interface plane that is attributable to the zero-momentum component of the transverse wave function). At the (100) surface of a cubic metal, states close to $\bar{\Gamma}$ that are predominantly s , p_z , and dz^2 -like have large zero-momentum fractions, while states close to $\bar{\Gamma}$ that are predominantly $px+py$, $dxz+dyz$, dx^2-y^2 and dxy -like have small zero momentum fractions. This is because symmetry considerations place no constraint on the zero-momentum fractions of s , p_z , and dz^2 -like states, while the zero-momentum fractions of $px+py$, $dxz+dyz$, $d(x^2-y^2)$ and dxy states are constrained by the symmetries of the basis functions to vanish at $\bar{\Gamma}$. Similar considerations apply to the other low-index surfaces.

The tetrahedral method for evaluating Brillouin zone integrals in density of states calculations is applied to calculate the external current in field emission from low-index metal-vacuum interfaces, based on self-consistent FP-LAPW calculations of the electronic structure. A calculation of the TED in field emission from $W(100)$ in the K -SDOS approximation failed to predict correctly the relative strengths of peaks of different symmetry. The present work shows that it is an excellent approximation to assume instead that the contribution of the higher-momentum components of the transverse wave functions is negligibly small.

The good overall agreement between the calculated TEDs of the field emission current from $W(100)$, $W(110)$, and $W(111)$ and the experimental data justifies the use of the present method to calculate also the surface densities of states and other features of the surface electronic structure. The Swanson hump on $W(100)$ results from the contribution of two flat bands of surface states at and around $\bar{\Gamma}$. The strong localization of charge just outside the surface of the metal results in a large electron flux at the interface plane, while the dz^2 symmetry results in a large zero-momentum component of the transverse wave function and hence a large contribution to the field emitted current. The widths of the Swanson hump measured at 78 K and at room temperature are closely equal, and significantly broader than that of the calculated peak, suggesting that the additional broadening is

a lifetime effect due to temperature-independent defect scattering. The calculated enhancement factor for $W(110)$ shows a weak peak at 0.6 eV below E_F . The fact that this peak is not clearly seen in the experimental enhancement factor is consistent with its inherent weakness together with lifetime broadening similar in magnitude to that on $W(100)$ in the same energy range. The $W(111)$ plane shows a strong asymmetric peak with its maximum at about 0.65 eV below E_F , which is due to a band of surface resonances of predominant d_{z^2} symmetry. Again, the discrepancy between the widths of peaks in the calculated TED and the experimental TED is consistent with Lorentzian broadening similar in magnitude to that inferred from the $W(100)$ data.

The present paper describes a method for calculating the field-emission currents from metallic surfaces, with and without ordered adsorbate overlayers, based on realistic treatments of their electronic and atomic structures. The present results for field emission from the low-index surfaces of clean tungsten demonstrate that this method can be used to extract information about surface states and surface resonances below the Fermi level from experimental field-

emission TEDs. This method, which is an adaptation of standard techniques for calculating the electronic properties of periodic structures and can readily be applied to a wide range of surfaces and materials, is capable of providing detailed information about the energies and symmetries of electronic states at metallic surfaces, the layer densities of states that play an important role in accounting for the distinctive chemical and optical properties of metallic surfaces, and changes in the electronic structure between the bulk metal and the surface. An extension to interpret photofield emission data from Ta has been reported elsewhere.²⁶

ACKNOWLEDGMENTS

We are indebted to J. C. L. Chow for help with the calculations, and to U. Birkenheuer and P. Blaha for helpful discussions. This work was supported in part by a Discovery Grant from the Natural Sciences and Engineering Research Council (NSERC) of Canada. One of us (Z. A. I.) wishes to acknowledge partial financial support from the University of Toronto, NSERC and the government of Ontario (OGS).

*Corresponding author. Electronic address:
lee@physics.utoronto.ca

- ¹D. R. Penn and E. W. Plummer, Phys. Rev. B **9**, 1216 (1974).
- ²S.-L. Weng, E. W. Plummer, and T. Gustafsson, Phys. Rev. B **18**, 1718 (1978).
- ³M. Posternak, H. Krakauer, A. J. Freeman, and D. D. Koelling, Phys. Rev. B **21**, 5601 (1980).
- ⁴L. W. Swanson and L. C. Crouser, Phys. Rev. Lett. **16**, 389 (1966).
- ⁵L. F. Mattheiss and D. R. Hamann, Phys. Rev. B **29**, 5372 (1983).
- ⁶S. Ohnishi, A. J. Freeman, and E. Wimmer, Phys. Rev. B **29**, 5267 (1984).
- ⁷S. B. Legoas, A. A. Araujo, B. Laks, A. B. Klautau, and S. Frota-Pessôa, Phys. Rev. B **61**, 10 417 (2000).
- ⁸Z. A. Ibrahim and M. J. G. Lee, Prog. Surf. Sci. **67**, 309 (2001).
- ⁹E. W. Plummer and J. W. Gadzuk, Phys. Rev. Lett. **25**, 1493 (1970).
- ¹⁰E. W. Plummer and A. E. Bell, J. Vac. Sci. Technol. **9**, 583 (1972).
- ¹¹A. Modinos and N. Nicolaou, Phys. Rev. B **13**, 1536 (1976).
- ¹²A. Modinos, *Field, Thermionic, and Secondary Electron Emission Spectroscopy* (Plenum, New York, 1984), Chap. 5.
- ¹³T. V. Vorburger, D. Penn, and E. W. Plummer, Surf. Sci. **48**, 417 (1975).

- ¹⁴Z. A. Ibrahim and M. J. G. Lee (unpublished).
- ¹⁵P. Blaha, K. Schwarz, G. Madsen, D. Kvasnicka, and J. Luitz, "WIEN2K, an augmented plane wave+local orbitals program for calculating crystal properties," Karlheinz Schwarz, Technical University of Wien, Austria, 2001.
- ¹⁶J. P. Perdew, J. A. Chevary, S. H. Vosko, K. A. Jackson, M. R. Pederson, D. J. Singh, and C. Fiolhais, Phys. Rev. B **46**, 6671 (1992).
- ¹⁷P. J. Donders, "Bulk effect photofield emission from tungsten," Ph.D. thesis, University of Toronto, 1988.
- ¹⁸N. D. Lang and W. Kohn, Phys. Rev. B **7**, 3541 (1973).
- ¹⁹R. G. Forbes, Ultramicroscopy **79**, 25 (1999).
- ²⁰R. D. Young, Phys. Rev. **113**, 110 (1959).
- ²¹P. E. Blochl, O. Jepsen, and O. K. Andersen, Phys. Rev. B **49**, 16 223 (1994).
- ²²J. P. Vigneron and Ph. Lambin, J. Phys. A **13**, 1135 (1980); Ph. Lambin and J. P. Vigneron, *ibid.* **14**, 1815 (1981).
- ²³H. Q. Nguyen, P. H. Cutler, T. E. Feuchtwang, and N. Miskovsky, Surf. Sci. **160**, 331 (1985).
- ²⁴D. Venus and M. J. G. Lee, Rev. Sci. Instrum. **56**, 1206 (1985).
- ²⁵G. S. Elliott, K. E. Smith, and S. D. Kevan, Phys. Rev. B **44**, 10 826 (1991).
- ²⁶T. Radon, P. Hądzel, M. J. G. Lee, Z. A. Ibrahim, and J. C.L. Chow, Surf. Sci. **549**, 103 (2004).